

A study of cascading failures in real and synthetic power grid topologies using DC power flows

Russell Spiewak,^{1,*} Sergey V. Buldyrev,¹ Yakir Forman,¹ Saleh Soltan,² and Gil Zussman²

¹Department of Physics,

Yeshiva University,

500 West 185th Street,

New York, NY 10033, USA

Email: {russell.spiewak,yakir.forman}@mail.yu.edu, buldyrev@yu.edu

²Department of Electrical Engineering,

Columbia University,

1300 S.W. Mudd

500 West 120th Street

New York, NY 10027, USA

Email: {saleh,gil}@ee.columbia.edu

(Dated: **June 10, 2021**)

Abstract

Using the linearized DC power flow model, we study cascading failures and their spatial and temporal properties in the US Western Interconnect (USWI) power grid. We also introduce the preferential Degree And Distance Attachment (DADA) model, with similar degree distributions, resistances, and currents to the USWI. We investigate the behavior of both grids resulting from the failure of a single line. We find that the DADA model and the USWI model react very similarly to that failure, and that their blackout characteristics resemble each other. In many cases, the failure of a single line can cause cascading failures, which impact the entire grid. We characterize the resilience of the grid by three parameters, the most important of which is tolerance α , which is the ratio of the maximal load a line can carry to its initial load. We characterize a blackout by its yield, which we define as the ratio of the final to the initial consumed currents. We find that if $\alpha \geq 2$, the probability of a large blackout occurring is very small. By contrast, in a broad range of $1 < \alpha < 2$, the initial failure of a single line can result, with a high probability, in cascading failures leading to a massive blackout with final yield less than 80%. The yield has a bimodal distribution typical of a first-order transition, i.e., the failure of a randomly selected line leads either to an insignificant current reduction or to a major blackout. We find that there is a latent period in the development of major blackouts during which few lines are overloaded, and the yield remains high. The duration of this latent period is proportional to the tolerance. The existence of the latent period suggests that intervention during early time steps of a cascade can significantly reduce the risk of a major blackout.

*Corresponding author

I. INTRODUCTION

The failure of a transmission line in a power grid leads to a redistribution of power flows in the grid. This redistribution may cause overloads of other lines and their subsequent failures, leading to a major blackout in a large area [6, 10, 24, 30]. These failures may be initiated by natural disasters, such as earthquakes, hurricanes, and solar flares, as well as by terrorist and electromagnetic pulse (EMP) attacks [33]. Recent blackouts, such as the 2003 and 2012 blackouts in the Northeastern US and in India [28, 29, 32], demonstrate that major power failure has a devastating impact on many aspects of modern life. Hence, there is a dire need to study the properties of cascading failures in power grids.

The studies of failures in power grids usually employ the direct current (DC) approximation of power flows [3, 7, 8, 11, 12, 15, 16, 25, 30]. In this paper, we employ a simplified DC model of a power grid which is equivalent to a resistor network [2] and follow the cascading failure model of [6, 30].

Ref. [11] suggests that the distribution of blackouts in power grids follows a power law, which is related to the phenomenon of self-organized criticality. Other authors suggest that blackouts follow first-order phase transitions, in which the loss of power is either very small or very large [24, 35]. The goal of this paper is to create a realistic model of a power grid which mimics the US Western Interconnect (USWI), to discover whether large blackouts can occur and to explore their distribution and spatial-temporal propagation, if they do occur. Additionally, we study the dependency of blackout characteristics on power grid design. For this reason, we introduce a synthetic Degree And Distance Attachment (DADA) model [20, 34].

We show that the characteristics of blackouts are universal. However, the sizes of blackouts are much smaller in the USWI-like model with a realistic design than in an artificial DADA model with a different spatial organization. In particular, we study how the size of the blackout and the dynamics of the cascading failures depend on a set of three parameters of the model which characterize the robustness of the grid: (1) tolerance α of the lines to overload, compared to their initial loads [21, 22]; (2) the minimum current I_p which any line in the network can carry independent of its initial load; and (3) the interval of currents of the transmission lines $I_{u-\Delta u}$ to I_u , from which a line is randomly selected to initiate the cascading failures. We characterize I_p and I_u by dimensionless parameters p and u : the level

of protection, $0 < p \leq 1$, and the significance of initial failure, $0 < u \leq 1$, which are the fraction of the lines with transmitting currents less than I_p and I_u , respectively.

We find that in a broad range of $1 \leq \alpha < 2$, $u \geq 0.8$, and $0 < p < 0.95$, large blackouts with final demand less than 80% of the initial demand may occur with a significant probability both in the USWI-like grid and in artificially constructed DADA grids. Moreover, we find that in this range of parameters the distribution of yield is bimodal, which is consistent with first-order phase transitions. Most importantly, we find that in each cascading failure which leads to a large blackout there is a latent period during which the damage is localized in space, few lines fail, and the decrease in yield is insignificant. The existence of this latent period suggests that the majority of blackouts can be effectively stopped by the timely intervention of grid operators. The length of the latent period increases as the tolerance α increases. Another important discovery is that in the event of a large blackout, cascading failures stop when the network breaks into small, disconnected islands.

The rest of the paper is organized as follows. In Section II we describe our methods of constructing power grids and simulating cascading failures. In Section III we study the properties of the USWI model and its cascading failures. Next, in Section IV we describe the preferential Degree And Distance Attachment (DADA) model. In Section V we compare the physical features and behavior of cascade simulations of the USWI model power grid and the DADA model. Finally, in Section VI we discuss and summarize the results of our study.

II. MODELS

In this section, we describe the network, flow model, and cascade model in detail.

A. Definition of the Grid Elements

We denote the set of all nodes as N and the set of all lines as E . Thus, a connected network is defined as the ordered pair $G = (N, E)$. We denote the power grid network by the graph G consisting of n^0 transmitting, n^+ supply, and n^- demand nodes. The total number of nodes is $n = n^0 + n^+ + n^-$. Each supply or demand node is specified by the amount of current it supplies ($I_i^+ > 0$) or by the amount of current it demands ($I_i^- > 0$). For transmitting nodes,

we assume $I_i^0 = 0$. Due to the law of charge conservation, $\sum I_i^+ = \sum I_i^-$. The network is specified by the $n \times n$ symmetric resistance matrix with elements R_{ij} , where R_{ij} is the resistance equivalent to the reactance value of the transmission line connecting nodes i and j . If there is no direct transmission line connecting nodes i and j , we assume that $R_{ij} = \infty$. Since the matrix with elements R_{ij} is symmetric, the total number of transmitting lines l is equal to the number of finite elements of the resistance matrix divided by two. Each node i is connected to k_i nodes by transmission lines, where k_i is the number of finite elements in the i^{th} row of the resistance matrix. Thus k_i represents the degree of node i and $\langle k \rangle$ is the average degree of all nodes in the network. We denote the set of all neighbors of node i as $N(i)$.

B. Flow Model

We employ the simplified DC model of a power grid widely used in the engineering community. This model is equivalent to flow equations in resistor networks. In this model the powers flowing through each line are replaced by currents, the reactances of each line are represented by resistances, and the phase angles are replaced by voltages. Each transmission line connecting nodes i and j is characterized by its resistance R_{ij} , while each node i is characterized by its voltage V_i . The current I_{ij} flowing from node i to node j is

$$I_{ij} = (V_i - V_j)/R_{ij}. \quad (1)$$

Additionally, the sum of all the currents flowing into each node i is equal to the sum of all currents flowing out:

$$\sum_{j \in N(i)} I_{ij} = \delta^+ I_i^+ - \delta^- I_i^-, \quad (2)$$

where $\delta_i^+ = 1$ or $\delta_i^- = 1$ if a node i is a supply or a demand node respectively, and $\delta_i^+ = \delta_i^- = 0$ otherwise. The particular methods used to solve the system of equations (1)-(2) can be found in Appendix A.

C. Cascading Failures Model

Once the system (1)-(2) is solved, we find the currents in all transmitting lines I_{ij} and define their maximum capacities I_{ij}^* using the following two rules (Fig. 1): (i) we define I_p as

the standard capacity of the lines. It is computed such that a fraction p of the lines initially have currents below I_p . We refer to p as the *level of protection*. (ii) For each line we define its individual capacity $\alpha|I_{ij}|$, where $\alpha \geq 1$ is the *tolerance* (i.e., the factor of safety). We assume α to be the same for every transmission line in the grid. Using these rules,

$$I_{ij}^* \equiv \max(I_p, \alpha|I_{ij}|). \quad (3)$$

If a current in line $\{ij\}$ exceeds I_{ij}^* , the line will fail.

The larger p and α are, the better the grid is protected against overloads. We usually use $p = 0.9$ and vary α as the main parameter of grid resilience. We introduce the standard capacity I_p because it would be unrealistic to assume that lines are built with very low capacity. In fact, many lines in realistic power grids may be built for backup reasons, so initially $I_{ij} = 0$. Without standard load requirements any redistribution of currents in the grid would lead to the failure of these backup lines, which contradicts their purpose.

To initiate a cascading failure, we randomly select and remove a single line for which the current $|I_{ij}|$ belongs to the interval of currents $[I_{u-\Delta u}, I_u]$, where the fraction $u - \Delta u$ of lines operate below $I_{u-\Delta u}$ and the fraction u of lines operate below I_u (Fig. 1). Throughout this paper we select $\Delta u = 0.1$. Precisely, the parameter u specifies the significance of the lines which are targeted for the initial failure. We refer to u as the *significance of initial failure*. For example, $u = 1.0$ and $\Delta u = 0.1$ means that the lines which initially fail are selected from the top 10% of lines ranked according to their initial current.

Real power grids are usually designed in such a way that the removal of a single element does not cause any instability in the system. This condition is called the $N - 1$ property. For simplicity, this model does not have the $N - 1$ property. However, removing a single line from a network without the $N - 1$ property is the equivalent to removing two lines from a network with the $N - 1$ property. Therefore, the properties of blackouts will be the same for networks without the $N - 1$ property as for networks with the $N - 1$ property, given equivalent line removals. The only difference is that the network with the $N - 1$ property will be more stable because the probability of simultaneous failure of two significant lines is much smaller than the probability of failure of one significant line.

It should be pointed out that removing a line can lead to disintegration of the grid into two disconnected components, which we call clusters. Obviously, the supply and demand in each cluster should be equalized to retain charge conservation. Thus, for each cluster C_j ,

Algorithm 1 Cascading Failures

Input: $G_0 = (N, E)$, α , p , u .

- 1: $E_0 \leftarrow E$.
 - 2: $\forall \{i, j\} \in E$ calculate I_{ij} .
 - 3: Determine I_p for given p .
 - 4: Choose a line $\{i, j\}$ from the interval $[I_{u-\Delta u}, I_u]$ of currents to fail; $s \leftarrow 0$, $F_0 \leftarrow \{i, j\}$ (s is stage of cascade; F_s is set of lines failed during s^{th} stage of the cascade).
 - 5: **while** $F_s \neq \emptyset$ **do**
 - 6: **for** each cluster C **do**
 - 7: Calculate $\sum_{i \in C} I_i^{+(s-1)}$ and $\sum_{i \in C} I_i^{-(s-1)}$.
 - 8: **if** $\sum_{i \in C} I_i^{+(s-1)} > \sum_{i \in C} I_i^{-(s-1)}$ **then**
 - 9: $\forall i: I_i^{+(s)} \leftarrow I_i^{+(s-1)} * \left(\frac{\sum_{i \in C} I_i^{-(s-1)}}{\sum_{i \in C} I_i^{+(s-1)}} \right)$
 - 10: **else if** $\sum_i I_i^{-(s)} > \sum_i I_i^{+(s)}$ **then**
 - 11: $\forall i: I_i^{-(s)} \leftarrow I_i^{-(s-1)} * \left(\frac{\sum_{i \in C} I_i^{+(s-1)}}{\sum_{i \in C} I_i^{-(s-1)}} \right)$
 - 12: **end if**
 - 13: **end for**
 - 14: $E_{s+1} \leftarrow E_s \setminus F_s$.
 - 15: $G_{s+1} \leftarrow G_s$ (G_s is the state of the grid at the s^{th} stage of the cascade).
 - 16: **for all** $\{i, j\} \in E_s$ **do**
 - 17: Calculate $I_{ij}^{(s)}$.
 - 18: **if** $|I_{ij}^{(s)}| > I_{ij}^*$ **then**
 - 19: $F_{s+1} \leftarrow F_{s+1} \cup \{i, j\}$.
 - 20: $G_{s+1} \leftarrow G_{s+1} \setminus \{i, j\}$.
 - 21: **end if**
 - 22: **end for**
 - 23: $s \leftarrow s + 1$.
 - 24: **end while**
-

we compute $\sum_{i \in C_j} I_i^+$ and $\sum_{i \in C_j} I_i^-$. If in a cluster $\sum_{i \in C_j} I_i^+ > \sum_{i \in C_j} I_i^-$, we multiply the current of each supply node in C_j by $\sum_{i \in C_j} I_i^- / \sum_{i \in C_j} I_i^+ < 1$; if $\sum_{i \in C_j} I_i^- > \sum_{i \in C_j} I_i^+$, we multiply the current of each demand node in C_j by $\sum_{i \in C_j} I_i^+ / \sum_{i \in C_j} I_i^- < 1$ (see Algorithm 1.6). In this equalization method, we spread the decrease in current uniformly among all the supply or demand nodes in C_j .

Then, we modify Eqs. (1)-(2), solve the resulting system of equations, and find new potentials $V_i^{(1)}$ and new currents $I_{ij}^{(1)}$. We also compute the total number of surviving lines $l_1 = l - 1$ and the total supplied current $I_1 = \sum_i I_i^{+(1)} = \sum_i I_i^{- (1)}$, where $I_i^{+(1)}$ and $I_i^{- (1)}$ are the new supply and demand currents, computed as described above if clusterization has occurred. We define this situation as the first time step $t = 1$ of the cascade of failures.

At the second time step of the cascade, we remove all lines for which the new current $|I_{ij}^{(1)}|$ exceeds the predefined maximum load of this line, I_{ij}^* . If no overloads have occurred, the cascade has stopped and we assume $I_f = I_1$ to be the final demand current of the process. If some of the lines fail, we repeat the equalization algorithm, modify the system of equations (1)-(2), calculate $V_i^{(2)}$ and new currents $I_{ij}^{(2)}$, and compute the new total demand current I_2 and the new total number of active lines l_2 .

We repeat this process recurrently until at a certain time step t of the cascade no lines fail. We call this time step the final time step of the cascade, and compute $I_f = I_t$, $l_f = l_t$, and the duration of the cascade $f = t$. The cascading failures algorithm is summarized in Algorithm 1.

D. Metrics

We define here all the metrics we use to characterize the cascades of failures.

Cascade Duration, f : the number of time steps until a cascade stops.

Number of Active Lines, $L = l_f$: the number of transmission lines in the grid that have not failed by the end of the cascade.

Yield, $Y(t)$: $\frac{I_t}{I_0}$, the ratio between the demand at time step t (I_t) and the original demand (I_0). For $t = f$, we simply denote yield by Y .

Large Blackout: $Y \leq 0.8$, when the yield in the grid drops below the threshold of 80%.

Risk of Large Blackout, $\Pi(\alpha)$: the probability that the failure of a line will produce a Large Blackout with $Y < 0.8$.

Table 1. Parameters of the model	
n^+	The number of supply nodes
n^-	The number of demand nodes
n^0	The number of transmitting nodes
I_i^+	The current supplied by supply node i
I_i^-	The current demanded by demand node i
R_{ij}	The resistance of the line connecting nodes i and j
V_i	The voltage of node i
I_{ij}	The current traveling through the line connecting nodes i and j
α	The tolerance of the lines
p	The level of protection of the lines
u	The significance of the initial failure

$\langle G \rangle$: the average relative size (fraction of nodes) of the largest cluster at the end of the cascade.

$\langle Y \rangle$: the average yield at the end of the cascade.

$\langle L \rangle$: the average number of surviving lines at the end of the cascade.

Hop distance, h_i : the shortest path measured in number of lines required to reach a certain node i from the failed line.

Local Yield, $Y(t, h)$:

$$Y(t, h) = \frac{\sum_{i \in H(h)} I_i^{-(t)}}{\sum_{i \in H(h)} I_i^-} \quad (4)$$

where $H(h)$ is the subset of demand nodes a given hop distance h from the failed line.

Blackout Radius of Gyration, $r_B(t)$: a quantitative measure of the blackout's geometric dimension as a function of the cascade time step t ,

$$r_B(t)^2 = \frac{\left\langle \sum_{i \in B(t)} h_i^2 I_i^{-(t)} \right\rangle}{\left\langle \sum_{i \in B(t)} I_i^- \right\rangle}, \quad (5)$$

where the summation is made over the set $B(t)$ of totally disconnected demand nodes which do not receive any current at the t^{th} time step of the cascade. The average is done either over all runs resulting in a large blackout or all runs not resulting in a large blackout.

t_l : duration of the latent period, i.e., the time step of the cascade of failures at which $Y(t_l)$ drops below 95%.

III. CASCADES IN USWI

In this section we simulate the cascades on the USWI network obtained from [6]. The network is based on real power grid topology data of the western US taken from the Platts Geographic Information System (GIS) [26] and includes approximate information about transmission lines based on their lengths, supplies based on power plants' capacities, and demands based on the population at each location.

A. USWI Properties

The USWI power grid data contains 8050 transmitting nodes, 1197 supply nodes, 3888 demand nodes, and 17544 transmission lines connecting them. To avoid exposing possible vulnerabilities in the actual USWI, our data set does not include the geographic coordinates of nodes. It does, however, include the length of each line r_{ij} connecting nodes i and j . We define the resistances of the lines to be proportional to their lengths $R_{ij} = \rho r_{ij}$, where ρ is a constant. The data set also specifies the supply (I_i^+) and demand (I_i^-) of each relevant node.

1. Degree Distribution

The USWI power grid is characterized by a fat-tail degree distribution of nodes (Fig. 2(a)), which can be approximated by a power law $P(k) \approx k^{-3}$ with an exponential cut-off. The degree distributions of transmitting nodes, supply nodes, and demand nodes are quite similar to each other (Fig. 2(a)). The average degree $\langle k \rangle$ of the nodes in the USWI is 2.67. For supply nodes, it is slightly larger (2.88); for demand nodes, it is very slightly smaller (2.61).

2. Length Distribution

The length distribution of lines for the USWI has an approximately lognormal shape with power law tails. Figure 3(a) shows $\ln P(\ln r_{ij})$, the logarithm of the probability density function (PDF) of $\ln r_{ij}$. For the lognormal distribution the graph would be a perfect parabola. Instead, we see that both tails of the distribution can be well approximated by straight lines with slope $\nu_- = 0.77$ for the left tail and slope $\nu_+ = -1.44$ for the right tail. This means that the PDF of r_{ij} can be approximated by power laws $P(r) \approx r^{\nu_- - 1}$ for $r \rightarrow 0$ and $P(r) \approx r^{\nu_+ - 1}$ for $r \rightarrow \infty$. The extra term -1 comes from the equivalence of cumulative distribution functions $P(r > r_0) = P(\ln r > \ln r_0)$, from which, differentiating with respect to r_0 , we obtain $P(r_0) = P(\ln r_0) d \ln(r_0) / dr_0 = P(\ln(r_0)) / r_0$.

A very small power for the left tail indicates an intriguing possibility that the USWI forms a fractal set with fractal dimension $D = 0.77 < 2$. Indeed, if the mass (number of nodes) within a circle of radius r scales as ar^D , it follows from the Poisson distribution that the probability to find an empty circle of radius r surrounding a given power station is $\exp(-ar^D)$. The derivative of this function is $\sim r^{D-1}$ for $r \rightarrow 0$. This is the probability density of the distances to the nearest neighbors, which should be a good approximation to the left tail of $P(r)$. Accordingly, the slope of the left tail $\nu_- = D$. The fractality of the population distribution was suggested in a number of works [4, 19]. This is particularly plausible for the US western regions, in which densely populated areas are separated by deserts and mountains.

3. Distribution of Supply, Demand, and Line Currents

The supplies (demands) in the USWI approximately follow a lognormal distribution, with a sharp cut-off in the right tail, indicating the existence of a technical upper limit for the supplies (demands) (see Fig. 4). Using this data we solve equations (1)-(2) and find the currents of transmission lines I_{ij} . The cumulative distribution function of currents in the USWI model is roughly exponential (Fig. 5), with about 10% extremely small currents.

B. Properties of Cascades in USWI

1. Bimodality of the Yield Distribution

The most important metric for studying cascading failures is the yield \mathbf{Y} . The yield critically depends on the initially failed line. We fix parameters of the model (α and p) and simulate the cascade initiated by the failure of a line selected from an interval of currents $[I_{u-\Delta u}, I_u]$. We measure yield and repeat this procedure $Q = 100$ times. Next we construct the histogram of yields.

The interesting feature of the yield histogram is its pronounced bimodality (Fig. 6(a)), which can be detected by a plateau in the cumulative yield distribution (Fig. 7(a)). The bimodality of the yield distribution is present in a large region of the parameter space (α, p, u) , characterized by relatively small $\alpha < 2$, practically all $p \leq 0.95$, and relatively large $u > 0.8$. The tolerance parameter α is identical to the tolerance $\alpha + 1$ of the Motter model [21, 22]. We find the same general behavior as in the Motter model, that as α increases the probability of a large blackout decreases (Fig. 7(a)).

One can see (Fig. 7(a)) that the distribution of yield clearly remains bimodal for $\alpha < 2$ for the USWI model. Similar behavior can be observed in the Motter model and the mutual percolation model, where the collapse transition is shown to be a first-order transition (all-or-nothing transition) [10, 18, 21, 22, 35]. In Section IID we defined large blackouts as having $Y < 0.8$. The motivation behind this definition is that there is a gap in the cumulative distribution of the yield between $Y = Y_1$ and $Y = Y_2$ that separates severe cascades from mild ones. It is possible to select $Y_m = 0.8$ as a value of Y that belongs to the interval $[Y_1(\alpha, p, u), Y_2(\alpha, p, u)]$ for a large section of the parameter space where the bimodality is observed. Thus this value can be used as a universal threshold which separates severe blackouts from mild blackouts. For large α , the gap in the yield distribution reduces and eventually disappears for $\alpha \geq 2$.

2. Risk of Large Blackouts

The ensemble of cascades can be characterized by two important parameters of the outcome: (i) the probability of a large blackout $P(Y < 0.8)$, which we call the risk of a large blackout $\Pi(\alpha)$, and (ii) the average blackout yield $\langle Y \rangle$, for the cases of large blackouts.

Figs. 8(a) and 8(b) show how the risk of large blackouts $\Pi(\alpha)$ decreases as α increases for different values of u and p . We find that for different values of u and p , the shapes of the curves $\Pi(\alpha)$ remain approximately constant, but the curves significantly shift in a horizontal direction. This means that the curves $\Pi(\alpha)$ can be well approximated by $\Pi(\alpha - \alpha_0(u, p))$. The function $\alpha_0(u, p)$ can be defined by solving the equation $\Pi(\alpha_0(u, p)) = 1/2$ with respect to $\alpha_0(u, p)$. One can see that $\alpha_0(u, p = 0.5)$ is an approximately linear function of u , which increases with u (Fig. 9(a)). This means that the higher the current of the initially failed line, the larger the tolerance necessary to achieve the same degree of protection for the transmission lines. In other words, the same effect can be achieved either by protecting a certain fraction of the most significant lines from spontaneous failure, or by increasing the tolerance of all the lines by some quantity (Fig. 9(a)). The dependence of the risk on p is weaker than on u , especially for $p \leq 0.5$ (Fig. 9(b)). An increase in p has practically no effect on increasing the robustness of the grid. The increase in p achieves a significant effect on the risk of large blackouts only when p approaches 0.9.

3. Characteristics of Large Blackouts

Large blackouts can be characterized by their average yield $\langle Y \rangle$, average fraction of surviving lines $\langle L \rangle$, and the average fraction of nodes in the largest connected component of the grid $\langle G \rangle$. These metrics only weakly depend on u , but are strongly increasing functions of α (Fig. 10(a)). The independence of the characteristics of large blackouts on u stems from the fact that the properties of large blackouts, if they occur, do not depend on a particular line to initiate the failure. The risk of large blackouts depends on u , but the average parameters of large blackouts do not.

The dependence of these metrics on p is more complex (Fig. 10(b)). While the yield $\langle Y \rangle$ starts to increase only for $p > 0.7$, the number of survived lines $\langle L \rangle$ significantly increases with p even for small p . This is not surprising since p is the level of protection of the lines, and fewer lines fail if more lines are protected. As p approaches 1, the dependence of $\langle L \rangle$ on α becomes very weak. The explanation of this fact is based on the notion that $\langle L \rangle$ is computed only for the case of *large* blackouts. For a large blackout to occur, a significant fraction of lines must fail, sufficient to disconnect a large fraction of demand nodes. On the other hand, as α increases, the risk of a large blackout decreases to zero, so the average

fraction of lines surviving for all the cascades (large and small) approaches 1.

Another important observation from Fig. 10(b) is the very small dependence of $\langle G \rangle$ on the parameters α , p , and u , as opposed to $\langle L \rangle$. Hence, by removing a small fraction of the lines (20%) the grid disintegrates into many small clusters, each less than 20% of the total size. Indeed, percolation theory predicts that close to the percolation threshold, it is sufficient to delete an infinitesimally small fraction of the so called “red” bonds (which form a fractal set with fractal dimension $3/4$) to divide the network into a set of small disconnected components [14].

C. Latent Period of the Cascade

The cascading failures that do not result in large blackouts ($Y > 0.8$) are usually short ($f < 8$) (Figs. 11(a) and 11(b)). In contrast, the duration of cascades resulting in large blackouts $Y \leq 0.8$ increases with α , reaching values of order 40 for large α . This means that for large tolerances, it takes much longer for the blackout to spread over a large area, since at each time step only a few lines have a huge overload and fail.

In the cascades resulting in large blackouts, the fraction of the consumed current, $Y(t)$, decreases with time in a non-trivial way (Fig. 12(a)). During the first few time steps of the cascades, the yield does not significantly decrease since the current can successfully redistribute over the remaining lines without disconnection of the demand nodes. This period, in which the cascade is still localized and a blackout has not yet occurred, can be called the *latent period of the cascade*. The recognition of this latent period is important since it is a period in which a cascade is beginning to spread but has not yet grown uncontrollable. In the latent period it may still be possible to intervene and redistribute current flow to stop the cascade before it becomes a large blackout.

We define the duration of this latent period of the cascade as the time step at which the yield drops below 0.95. At approximately this time step the yield starts to rapidly decrease and then, towards the end of the cascade, stabilizes again. The shape of this function is characteristic of an abrupt first-order transition observed in simpler models of network failure [10, 22]. Remarkably, the duration of the latent period is a linear function of tolerance (Fig. 12(b)).

D. Cascade Spatial Spreading

To observe the spatial spread of the reduction of demand for each run, we group the grid’s demand nodes into bins based on their “hop distance” from the original failed line. In each bin we compute the local yield $Y(t, h)$. We average the local yield $Y(t, h)$ for runs resulting in large blackouts (Fig. 13(a)). The yield in each bin at the end of cascades resulting in large blackouts is almost independent of the distance from the initially failed line. While at the beginning of the cascade the blackout is localized near the initially failed line, eventually the blackout spreads uniformly over the entire system. Delocalization occurs at the end of the latent period of the cascade. This can be clearly seen from the behavior of the blackout profiles, which start to rapidly drop down for large distances only at intermediate time steps of the cascade.

To give a more quantitative measure of the blackout spread, we use the “blackout radius of gyration” ($r_B(t)$) metric defined in Section IID. Fig. 14 shows the behavior of $r_B(t)^2$ versus the cascade time step t for the cascades which result in small blackouts (Fig. 14(a)) and large blackouts (Fig. 14(b)). We observe the same phenomena — initially $r_B(t)^2$ grows slowly in the runs resulting in large and small blackouts. However, while in runs resulting in small blackouts the cascade stops during this latent period, in runs resulting in large blackouts the cascade starts to rapidly spread over a large area. It should still be noted, though, that the rate of this spread decreases when tolerance increases.

E. Main Lessons Learned from the Cascades in the USWI model

1. The yield has a pronounced bimodality, for which a grid suffers either a large blackout with $Y < 80\%$ or a very small reduction of demand with $Y > 90\%$.
2. Increasing tolerance α decreases the probability $\Pi(\alpha)$ of a large cascade with low yield.
3. The higher the significance of the initially failed line u , the larger the tolerance α necessary to prevent cascades. Thus, the same effect can be achieved by protecting a certain fraction of the most important lines from spontaneous failure as by increasing the tolerance α of all lines.
4. $\langle Y \rangle$ strongly depends on α and weakly depends on u . It increases with p for only

$p > 0.7$.

5. $\langle L \rangle$ also strongly depends on α and weakly depends on u . It increases with p even for small p .
6. $\langle G \rangle$ weakly depends on α and practically does not depend on p and u . This suggests that in large blackouts the grid disintegrates into very small clusters.
7. Cascades which do not result in large blackouts are usually short. Cascades resulting in large blackouts usually take a large number of time steps, and the number of time steps increases with α .
8. There is a latent period during which the reduction in demand is small and not many lines have failed. During this period, it may be possible to intervene and optimally redistribute current flow to prevent the cascade from growing uncontrollable and to prevent a large blackout. The duration of the latent period linearly increases with α .
9. In cascades resulting in large blackouts, the reduction in demand usually begins in the vicinity of the initially failed line and the blackout remains localized near the initially failed line until the end of the latent period.
10. For cascades resulting in large blackouts, the final local yield is almost independent of the distance from the initially failed line.

IV. DEGREE AND DISTANCE ATTACHMENT MODEL

In the previous section we find that cascading failures in the USWI model have characteristic features of a first-order transition: the bimodal distribution of yield and the latent period during which the damage to the network is insignificant. It is important to investigate whether these features are due to particular characteristics of the USWI design, or whether they are universal features of a much broader class of models. Moreover, the data on real grids are limited and therefore it is important to develop algorithms for generating synthetic grids resembling known real grids. The two basic features of USWI that we would like to reproduce are the degree distribution and the distribution of line lengths. The degree distribution of the USWI discussed in Section III is in agreement with the Barabási-Albert

preferential attachment model [1, 5]. Accordingly we use the Barabási-Albert model as the basis of the synthetic model. In the original Barabási-Albert model, a newly created node is attached to an existing node with a probability proportional to the degree of this node. However, for power grids embedded in two-dimensional space, the length distribution of lines, resulting from the degree preferential attachment, would not decrease with the length. Therefore, in order to create a grid with a decreasing length distribution, one must introduce a penalty for attaching to a distant node. Here we will employ the Degree And Distance Attachment (DADA) model with a distance penalty developed in Refs. [20, 34]. This method produces degree and length distributions similar to those of the USWI (see Section III A).

The DADA model randomly generates nodes $j = 1, 2, \dots, n$ on a plane with a uniform density one by one. It connects each new node j to an existing node i based on i 's degree and distance with probability $P(\{i, j\}) \propto k_i/r_{ij}^\mu$, where k_i is a current degree of node i and r_{ij} is the distance between nodes i and j . This rule mimics the way real networks are evolved. A real network such as the USWI is not planned all at once; rather, new stations are added to the grid as necessity dictates. The probability of connection $P(\{i, j\}) \propto k_i/r_{ij}^\mu$ is assumed to be proportional to k_i , since connections to nodes of high degree are more reliable, but also inversely proportional to a power of r_{ij} , since construction of long transmission lines costs more. The distance penalty μ is a factor which seeks to optimize the balance between reliability and cost (see Algorithm 2.21). As in USWI, we assume that in the DADA model $R_{ij} = \rho r_{ij}$, where ρ is resistivity, which is constant for all the lines in the system.

Refs. [20, 34] show that for $\mu < 1$, the degree distribution of the DADA model is a power law $P(k) \approx k^{-3}$, while for $\mu > 1$, it becomes a stretched exponential [13]. However, the fat-tail of the stretched exponential can be approximated by a power law $P(k) \approx k^{-\gamma}$ with an exponent $\gamma > 3$ (Fig. 2(b)). Ref. [20] also shows that the line length distribution $P(r_{ij}) \approx r_{ij}$ for $r_{ij} \rightarrow 0$, and for large μ , $P(r_{ij}) \approx r_{ij}^{-3}$ for $r_{ij} \rightarrow \infty$. The functional form of $P(r_{ij})$ for the DADA and USWI models are similar, but the exponents are different. As mentioned in Section III A 2 regarding the USWI model, these asymptotic behaviors correspond to the slopes $\nu_- = 2$ and $\nu_+ = -2$ of the logarithmic distribution $P(\ln(r_{ij}))$ observed in the DADA model (Fig. 3(b)), while for the USWI model these values are $\nu_- = 0.77$ and $\nu_+ = -1.43$. In our simulations, we select $\mu = 6$. For this choice of μ , the degree distribution exponent $\gamma \approx 4.3$, while $-\nu_+ = 2$. The corresponding values in the USWI model are smaller. Both γ and $-\nu_+$ can be decreased by decreasing μ , so that the degree and length distributions

of the DADA model would be closer to those of the USWI. However, upon doing so, our results on the distribution of currents in the DADA model and properties of the cascading failures do not change significantly, indicating that the observed features of the cascades are quite universal. The discrepancy in ν_- for the DADA and USWI is related to the fact that in the DADA model the nodes are spread on the plane with a uniform density, while in the USWI model the density of nodes is related to the population density which has fractal-like features.

A. Construction of the DADA model

In this subsection, we will describe in detail the construction of the DADA model [20, 34]. We generate the coordinates (x_i, y_i) of n nodes randomly with a homogeneous density n/S^2 over the $(S \times S)$ square with periodic boundary conditions. For this periodic square, the distance r_{ij} between two points with coordinates (x_i, y_i) and (x_j, y_j) is computed as

$$r_{ij} = \sqrt{\Delta x^2 + \Delta y^2}, \quad (6)$$

where $\Delta x = \min(|x_i - x_j|, |S - |x_i - x_j||)$ and $\Delta y = \min(|y_i - y_j|, |S - |y_i - y_j||)$. We select $S = 1$. Periodic boundary conditions are often used in statistical physics to minimize finite size effects [27]. Our goal is to create a grid with a given number of lines, l . We start by randomly placing nodes onto the grid one by one until we have a total of n nodes (see Algorithm 2.3). When each new node is created, we connect it on average to $\bar{\ell} = l/n = \langle k \rangle / 2$ preexisting nodes in order to achieve our goal of creating a grid with a given number of lines l . Since $\bar{\ell}$ is a real number, we preassign to each node i an integer ℓ_i , the number of lines by which it will be connected to the previously generated nodes, according to Algorithm 2.4. We randomly select $l - n[\bar{\ell}] < n$ nodes, where $[\bar{\ell}]$ is the integer part of $\bar{\ell}$. For these nodes, we choose $\ell_i = [\bar{\ell}] + 1$. For the rest of the nodes, we choose $\ell_i = [\bar{\ell}]$. For each new node j , we attempt to create ℓ_j lines with the previously existing nodes. If $j \leq \ell_j$, then we connect j to all preexisting nodes (see Algorithm 2.10), as we cannot create ℓ_j lines without duplicating lines. If $j \geq \ell_j$, there are more existing nodes than ℓ_j and we create lines according to the following rule (see Algorithm 2.17). First we compute the distances r_{ij} between the new node j and all existing nodes $i < j$ (see Algorithm 2.20). Next we assign to each existing node i a probability $P(\{i, j\})$ of connecting to the new node j , proportional to k_i/r_{ij}^μ , where

Algorithm 2 DADA Model Construction

```
1: Select a random subset  $\Lambda$  of size  $l - \bar{\ell}n$  from  $\{1, 2, \dots, n\}$ .
2: for  $j \leftarrow 1$  to  $n$  do
3:   Choose coordinates  $x_j$  and  $y_j$  between 0 and  $S$ .
4:   Choose integer number  $\ell_j$ :
5:   if  $j \in \Lambda$  then
6:      $\ell_j = \lfloor \bar{\ell} \rfloor + 1$ .
7:   else
8:      $\ell_j = \lfloor \bar{\ell} \rfloor$ .
9:   end if
10:  if  $j \leq \ell_j$  then
11:    for all  $i < j$  do
12:      Connect  $j$  to  $i$ .
13:    end for
14:     $k_j \leftarrow j - 1$ .
15:  else
16:     $k_j \leftarrow 0$ .
17:    while  $k_j < \ell_j$  do
18:      for all  $i < j$  do
19:        if  $j$  is not directly connected to  $i$  then
20:          Compute  $r_{ij}$ .
21:          Assign Probability  $P(\{i, j\}) \propto k_i / r_{ij}^\mu$ .
22:        else
23:           $P(\{i, j\}) = 0$ .
24:        end if
25:      end for
26:      Choose node  $i$  from distribution  $P(\{i, j\}) \propto k_i / r_{ij}^\mu$  and connect it to  $j$ .
27:       $k_j \leftarrow k_j + 1$ .
28:    end while
29:  end if
30: end for
31: return  $G$ .
```

k_i is the degree of node i and μ is a parameter giving the penalty for distance (see Algorithm 2.21). We then connect the new node to a node chosen from this probability distribution (see Algorithm 2.26). We repeat this step ℓ_j times, with the additional condition that all nodes i already directly connected to node j have probability of connecting $P(\{i, j\}) = 0$ instead of $P(\{i, j\}) \propto k_i/r_{ij}^\mu$ (see Algorithm 2.23). At the end, a total of almost $n\bar{\ell} = l$ lines are created.

For the USWI network $\bar{\ell} = \langle k \rangle / 2 \approx 1.5$, so for the DADA model we choose $\bar{\ell} = 1.5$ (more accurate values of $\bar{\ell}$ do not significantly affect our results). As mentioned in Section III, the average degree $\langle k \rangle$ of the USWI network is 2.67. For supply nodes, it is slightly larger (2.88); for demand nodes, it is very slightly smaller (2.61). Averaging over 100 different grids, our DADA model has slightly higher average degree of 2.84. More accurate values of $\bar{\ell}$ do not significantly change the cascading properties of the DADA model.

After placing n nodes and l lines, we randomly assign n^+ supply nodes and (different) n^- demand nodes. Our network was simulated with $n = 13135$, $n^- = 3888$, and $n^+ = 1197$ to match the USWI. We assign the supply and demand nodes independent of degree. Thus the average degrees of the supply and demand nodes are the same as the average degree of the DADA model.

Since the supplies and demands of the USWI have an approximately lognormal distribution (see Fig. 4), we generate currents of supplies and demands in the DADA model following a modified lognormal distribution:

$$I_i^+ = e^{\nu_i \sigma^+ + m^+ \ln k_i}, \quad (7)$$

for supplies and

$$I_i^- = e^{\nu_i \sigma^- + m^- \ln k_i}, \quad (8)$$

for demands, where ν_i is randomly generated according to a standard normal distribution, σ^\pm is a standard deviation, and m^\pm is a parameter which creates a correlation between the node's current and its degree.

Furthermore, since it is unrealistic to have nodes with very high supply and demand values, we introduce a cut-off $a^\pm \sigma^\pm$, where a^\pm is a parameter of the model such that we accept only $I_i^\pm \leq e^{a^\pm \sigma^\pm}$. Thus, the supply and demand of each node is

$$I_i^\pm = \min \left(e^{\nu_i \sigma^\pm + m^\pm \ln k_i}, e^{a^\pm \sigma^\pm} \right). \quad (9)$$

This cut-off corresponds to the sharp drops of the right tails of the supply and demand distributions in the USWI (Fig. 4).

To best match the USWI data, we let the values of m^\pm be the slopes of the regression lines of the log-log scatter plots which plot the average supply/demand versus the degree of corresponding nodes. We then select values of σ and a so that the distributions simulated for the DADA model best match the USWI distributions (Fig. 4). We obtain $\sigma^+ = 2.0$, $m^+ = 0.38924$, $a^+ = 1.6$, $\sigma^- = 1.8$, $m^- = 0.62826$, and $a^- = 1.2$.

V. COMPARISON OF THE USWI AND DADA MODELS

Here we compare the main results from the USWI model and the DADA model. We also discuss reasons for the differences observed. The cumulative distribution of currents in the DADA model closely follows the exponential distribution of currents in the USWI grid (Fig. 5). This is important because the ratio of currents in the two models corresponding to the same significance of lines u is approximately constant.

A. Evolution of Cascades

The distribution of the yield Y in the DADA model is also bimodal for approximately the same set of parameters α , u , and p as in the USWI model, but the gap between the two modes is significantly wider in the DADA model than in the USWI model (Fig. 7). Figure 7 compares the yield distributions of the USWI and DADA models for $u = 1$ and $p = 0.9$ for several values of $1 \leq \alpha < 2$. Both models always collapse ($Y < 0.8$) for small values of α , and survive ($Y > 0.8$) for large values of α . But for the DADA values, chances of large blackout (risk) are smaller for the same set of parameters than in the USWI model. For example, the DADA model can still survive with a small probability for $\alpha = 1.2$, but the USWI always collapses for $\alpha < 1.3$. Conversely, we do not observe any large blackouts in the DADA model for $\alpha > 1.7$, while the USWI model can still have large blackouts even for $\alpha = 1.9$. Thus, even though in the event of a large blackout the average yield in the USWI is greater than in the DADA model (and thus, in this sense, the DADA model is more vulnerable than the USWI model), the risk of large blackouts is greater in the USWI model than in the DADA model for the same set of parameters.

These differences may be related to the fractal structure of the USWI, in which densely populated areas with lot of demand and supply nodes are separated by large patches of empty land over which few long transmission lines are built, whereas the DADA model has constant density of nodes. Thus, it is less likely that the cascade will spread over the entire grid in the USWI model than in the DADA model, but a higher tolerance is necessary to prevent large blackouts in the USWI model than in the DADA model.

Qualitatively, the behaviors of the metrics $\langle Y \rangle$, $\langle L \rangle$, and $\langle G \rangle$ are similar in the USWI model and in the DADA model, but in the DADA model the survival quantities are always smaller for the same α , u , and p . This indicates that, remarkably, the artificial DADA model is more vulnerable than the USWI model based on actual data (Figs. 8, 9, and 10). The values of $\langle G \rangle$ in the DADA model are very small, indicating that in the event of a large blackout the DADA network disintegrates into very small connected components, each constituting about 1% of the nodes of the grid. In the USWI grid, the average largest component is larger, because USWI grid consists of several dense areas connected by few long lines. The overload of these long lines breaks the USWI grid into relatively large disconnected components, preventing the cascade from further spreading.

B. Cascade Temporal Dynamics

The spatial and temporal behaviors of the cascades in the DADA model closely follow the behaviors in the USWI model (Figs. 11, 12, 13, and 14). $r_B(t)^2$ in the DADA model is much smaller than in the USWI model due to the different structures of the models and difference in diameters of the networks. The longest distance (in terms of number of hops) between any two nodes (i.e. diameter of the network) in the DADA model is ≈ 16 , while in the USWI model it is ≈ 41 . In both models we see that the cascade spreads more quickly for smaller α than for larger α . However, the first-order all-or-nothing nature of the cascades, characterized by a latent period during which the blackout is small and localized followed by a fast blackout spread over a large area, is common in both models.

C. Cascade Spatial Spreading

The DADA model has an advantage over the USWI model, that in the former we know the exact coordinates of the nodes and thus we can illustrate the spatial and temporal evolution of the blackout as a sequence of snapshots on the (x, y) plane. Fig. 15 shows spatial snapshots of the cascading failures taken at different time steps for the DADA model with parameters $\alpha = 1.8$ and $p = 0.4$. The color of a line indicates the time step of the cascade at which this line has failed. One can see that during first 3 time steps of the cascade (red lines) the area of line failures is small and localized near the initial failure. The cascade starts to spread during time steps 4-8 (orange and yellow-green), but the area of line failures is still localized. At time step 10 the cascade quickly spreads to very distant parts of the system (green). The blue and violet lines are the final time steps of the cascade. Thus, the figure suggests that there is a latent period of the cascade during which the area of line failures is small and localized.

VI. CONCLUSION

The DADA model and the USWI model have many common features. The physical features, such as the distribution of degrees, resistances, and currents, compare well in both models. The behavior of the cascades of failures in the DADA model is also similar to their behavior in the USWI model power grid, despite the differences in construction of these models.

The overloads and cascading failures in the USWI and DADA models have features of all-or-nothing transition, just like in a broad spectrum of more primitive models such as the Motter model [21, 22]. In the Motter model, instead of currents, the betweenness of each node in a graph is computed and the maximum load of each node is defined as its original betweenness multiplied by the tolerance. Then, a random node is taken out, simulating an initial failure, and the new betweenness of each node is calculated. If the new betweenness of a node exceeds its maximum load, this node is taken out and the entire process is repeated. The yield in the Motter model is defined as the fraction of survived nodes at the end of the cascade. The distribution of the yield in the Motter model is bimodal for a large range of tolerances. Similarly, in a wide range of parameters, both the DADA model and the USWI

power grid are in a metastable state and there exists the risk that the failure of a single line will lead to a large blackout, in which the yield falls below 80%. As tolerance increases beyond 2.0, the risk of a large blackout decreases almost to 0.

The level of line protection, p , increases the robustness of the grid, but to a lesser extent than does the tolerance. An important parameter defining the robustness of the grid is the significance of the initial failure u . The risk of a large blackout increases with u in the same way as with tolerance. Given a particular α , when u is small, there is practically no risk of a large blackout, while when u approaches 1, the risk is maximal for the given α . If α is kept constant and u decreases, there is the same effect on the risk of a large blackout as when α increases and u is kept constant, meaning that the same effect could be achieved by protecting important lines as by increasing the overall tolerance. Nevertheless, even if the initially failed lines are selected irrespective of their currents ($u = \Delta u = 1$), the distribution of yields remains bimodal, but the probability of large blackouts significantly decreases.

Upon failure of a line, the first few cascade time steps affect only the immediate vicinity of the failed line. This is the latent period of the cascade, during which it may be feasible to intervene and redistribute the current flow and possibly prevent a large blackout from occurring. At some time step, the cascade may begin to spread quickly, and only then will a large blackout occur. In this case, the blackout radius increases rapidly with cascade time steps, but with a lower rate for higher values of α . Once the failure has spread over the entire grid, the cascade continues to overload a small number of lines before terminating. At this time step the grid completely disintegrates into small disconnected clusters. During the first few time steps of the cascade, the demand does not significantly decrease, but starts to quickly drop at the end of the latent period. The duration of the latent period of the cascade linearly increases with the overall tolerance and provides sufficient time for grid operators to intervene and stop the cascade.

Similar phenomena were observed during the large blackout of August 14th 2003. It is well documented [23] that the power outage, which affected a large portion of the Northeastern region of the USA on August 14th 2003, was caused by line overloads due to a heat-wave. But what might have been a manageable local blackout cascaded into massive widespread distress on the electric power grid. Power was not re-distributed after overloaded transmission lines hit unpruned foliage, and the spreading of blackout was exacerbated over a time period of 30 minutes. This example closely resembles the large blackout scenario predicted by our

models. Thus, our model provides useful understanding of general features of the cascades of failures in power grids, which may be used for increasing the resilience of power grids and designing optimal shedding strategies for preventing cascades from spreading.

VII. ACKNOWLEDGMENTS

This work was supported in part by DTRA grants HDTRA1-10-1-0014, HDTRA1-14-1-0017, and HDTRA1-13-1-0021, DARPA RADICS under contract #FA-8750-16-C-0054, DOE GMLC program, and the People Programme (Marie Curie Actions) of the European Unions Seventh Framework Programme (FP7/2007-2013) under REA grant agreement no. [PIIF-GA-2013-629740].¹¹ We also acknowledge the partial support of this research through the Dr. Bernard W. Gamson Computational Science Center at Yeshiva College. We thank Meric Uzunoglu and Andrey Bernstein for their help with processing the USWI data. We also thank Guifeng Su for his work on programming the preferential attachment algorithm and measuring “hop distance”, Yehuda Stuchins for his preliminary work on studying relations between distance and failures, and Tzvi Bennoff for testing alternative parameters. We appreciate the assistance of Adam Edelstein, Jonathan Jaroslawicz, and Brandon Bier in sorting the data. We are grateful to S. Havlin, G. Paul, and H.E. Stanley for productive interactions.

VIII. FIGURES

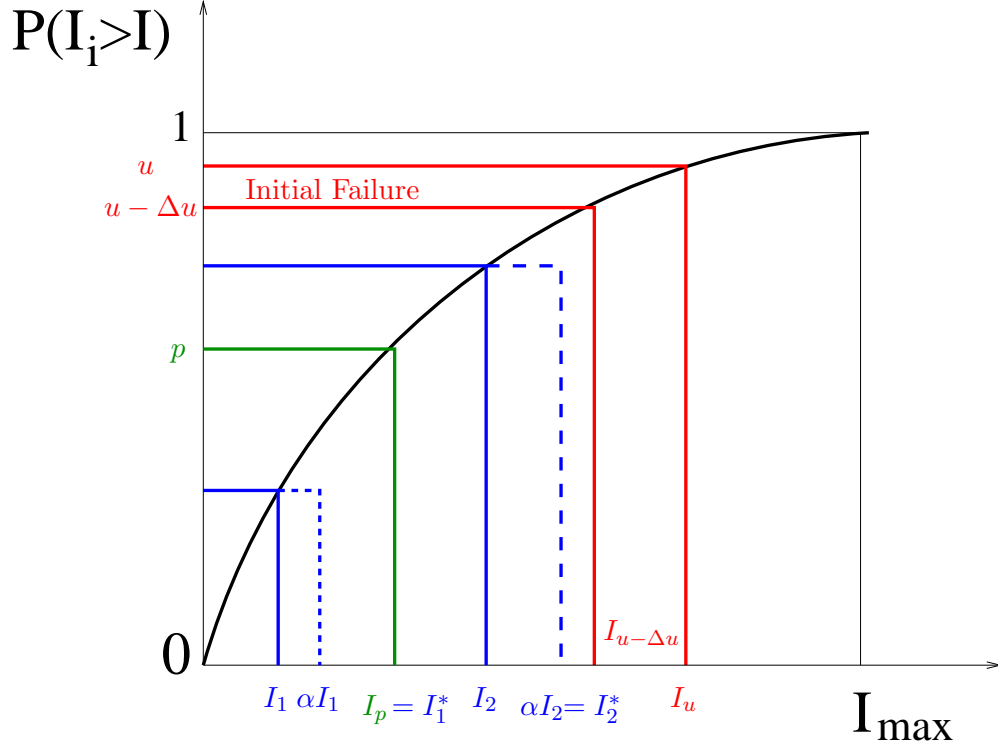


FIG. 1: (Color online) Schematic illustration of the rules of cascading failures. The black solid line represents the cumulative distribution of currents in transmission lines. The green solid line indicates the fraction p of uniformly protected lines and the current I_p corresponding to this fraction. Blue solid lines indicate the initial loads of two transmission lines I_1 and I_2 . Blue dashed lines indicate the maximum loads of these lines αI_1 and αI_2 , defined using the tolerance parameter α . Since $\alpha I_1 < I_p$, the actual maximum load for line 1 is I_p . In contrast, since $\alpha I_2 > I_p$, the actual maximum load for line 2 is αI_2 . Red lines show the maximum and the minimum fraction of lines, and their corresponding currents, from which region the initially failed lines can be selected for given parameters u and Δu .

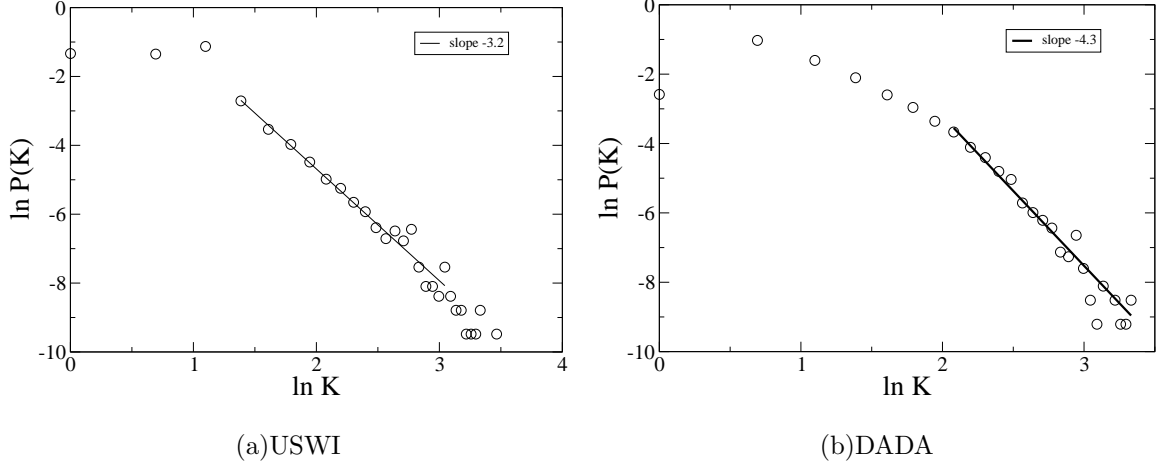


FIG. 2: Degree Distributions of (a): the USWI power grid, and (b): the DADA model for $\mu = 6$, $\ell = 1.5$.

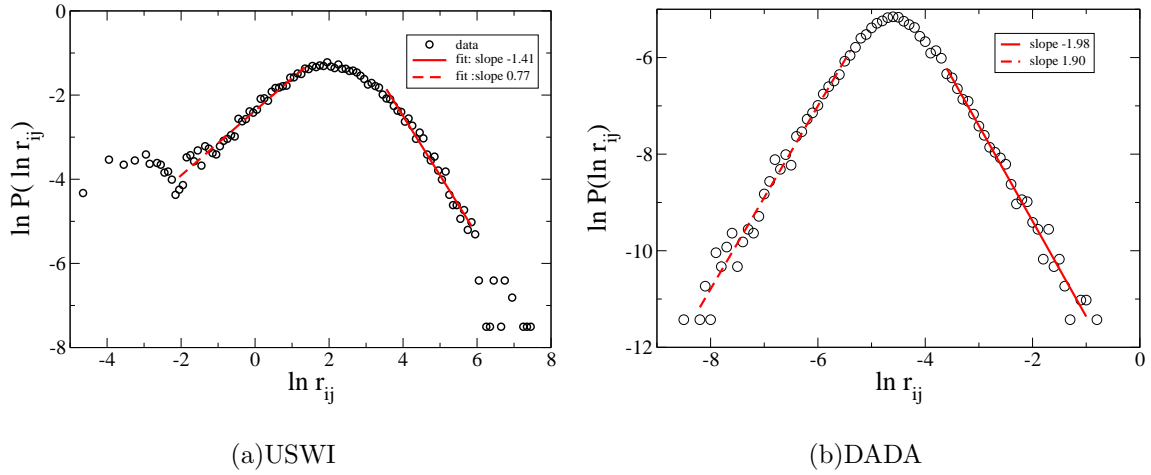


FIG. 3: Distribution of the line lengths, which are the same as resistances, in (a): the USWI power grid, and (b): the DADA with $\mu = 6$, $\ell = 1.5$.

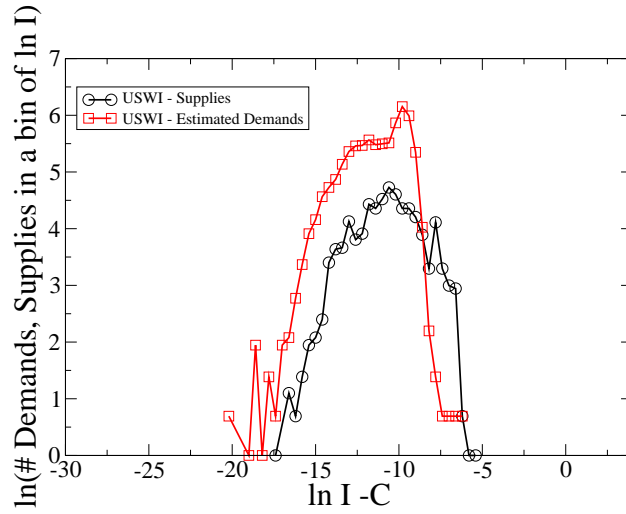


FIG. 4: Distribution of the supplied and demanded currents in the USWI power grid. Currents are portrayed in arbitrary units.

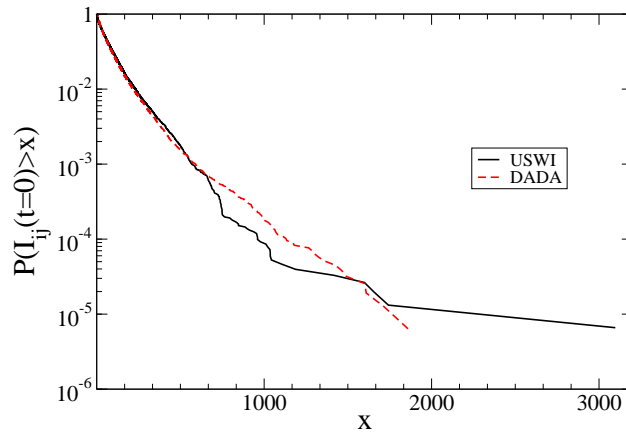


FIG. 5: Cumulative distribution of currents for the USWI model power grid and DADA model with $\mu = 6$ and $\ell = 1.5$. (Currents are measured in arbitrary units.)

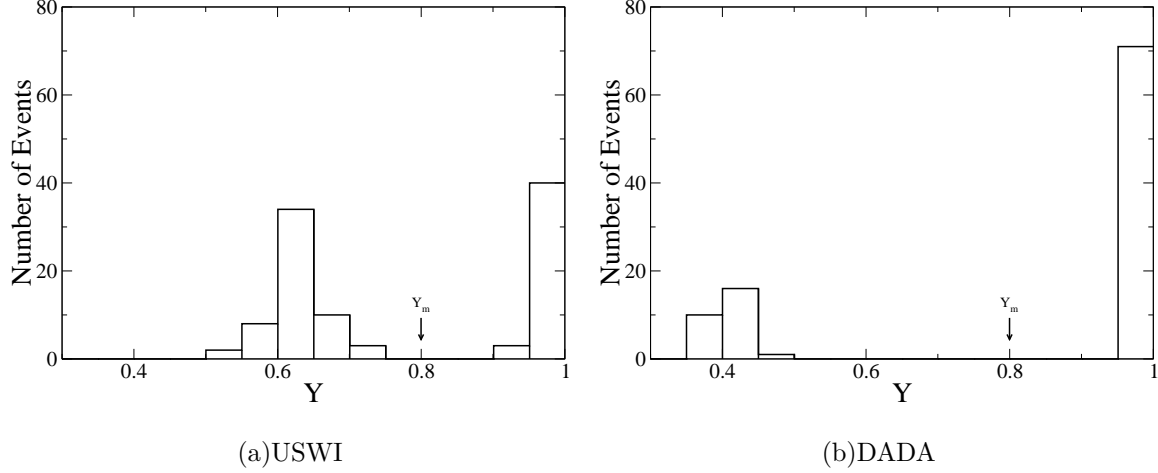


FIG. 6: Distribution of yield for $\alpha = 1.6$, $p = 0.9$, and $u = 1.0$. One can clearly see the bimodality of the distribution with two peaks for high yield 0.975 and low yield 0.625, with practically no yields between 0.75 and 0.9 for the USWI (a). Similarly for the DADA, one can clearly see the bimodality of the distribution with two peaks for high yield 0.975 and low yield 0.425, with practically no yields between 0.5 and 0.95 (b).

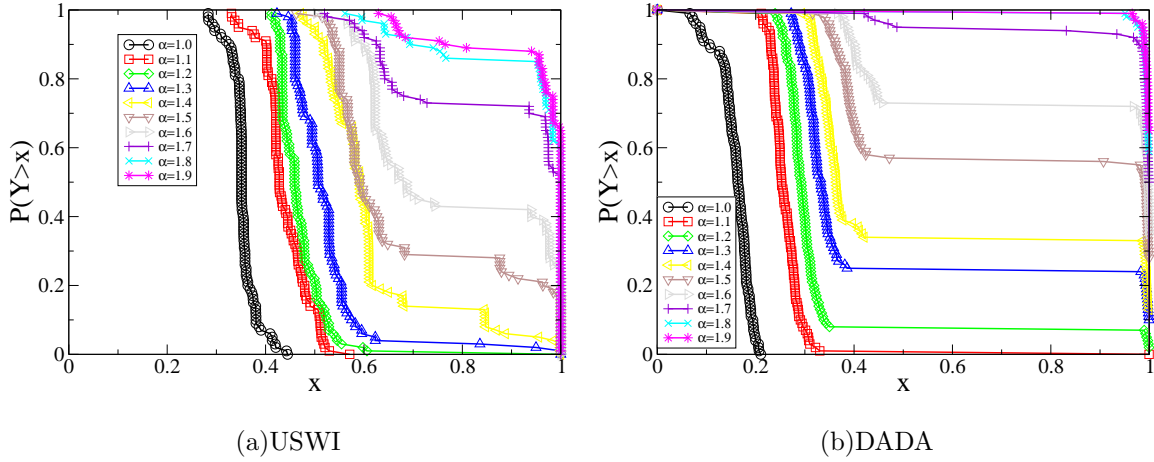
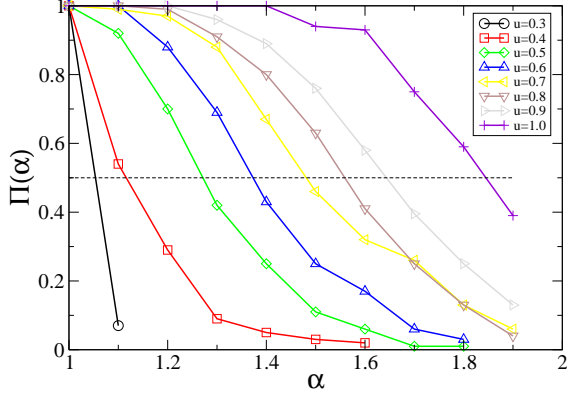
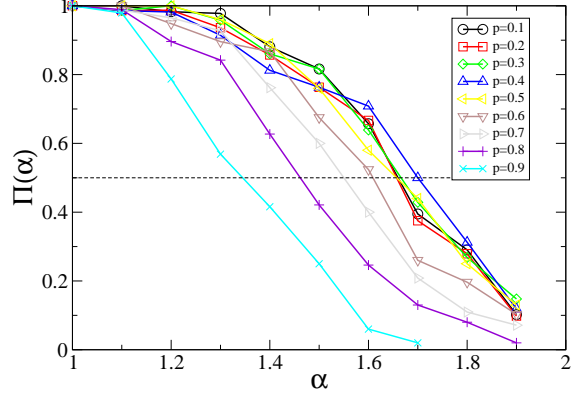


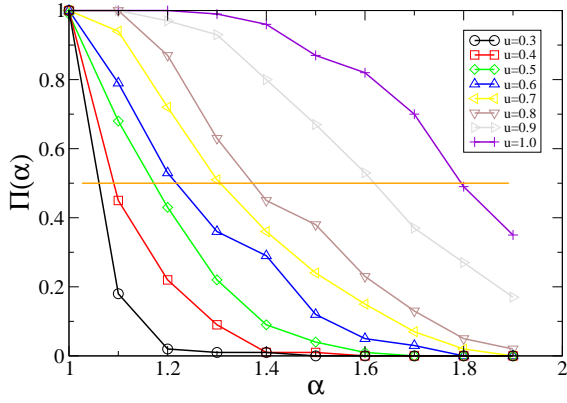
FIG. 7: Cumulative distribution of the yield for $p = 0.9$, $u = 1.0$ and various values of α for (a) the USWI model, and (b) the DADA model with $\mu = 6$, $\ell = 1.5$. The large gap in the distributions is a feature of the abrupt first-order transition. For the USWI, $u = 1.0$ means that the distribution is obtained by running 100 simulations with the initial removal of one of the top 100 lines with the largest initial currents.



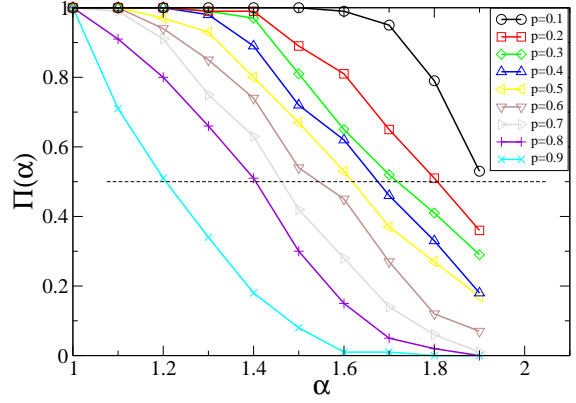
(a)USWI, $p = 0.5$



(b)USWI, $u = 0.9$



(c)DADA, $p = 0.5$



(d)DADA, $u = 0.9$

FIG. 8: Probability of large blackout $P(Y < 0.8)$, or risk $\Pi(\alpha)$, as function of α . (a) USWI model for different values of u and $p = 0.5$. (b) USWI model for different values of p and $u = 0.9$. (c) DADA model for different values of u and $p = 0.5$. (d) DADA model for different values of p and $u = 0.9$.

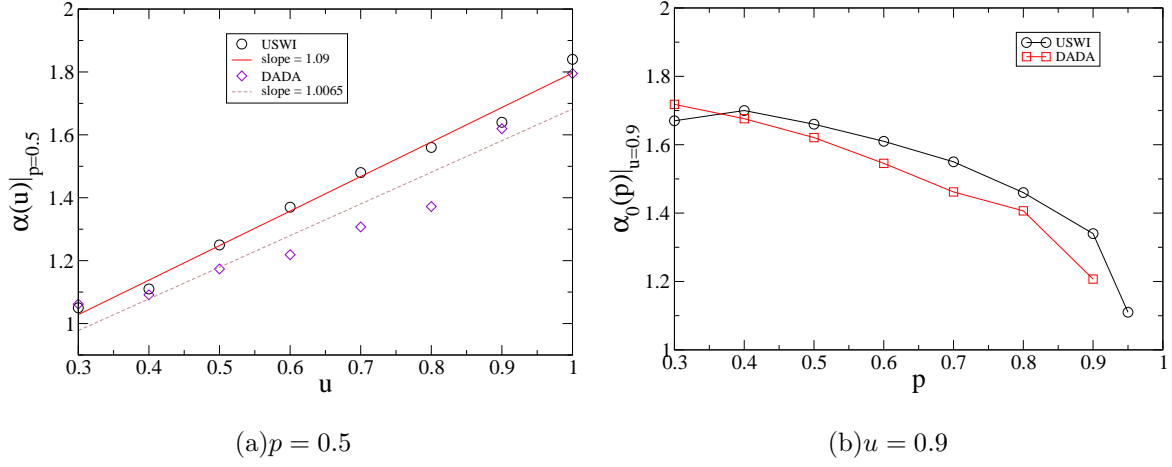


FIG. 9: Behavior of $\alpha_0(u, p)$ defined as the value of α such that $r(\alpha, u, p) = 0.5$ as function of u at constant $p = 0.5$ (a) and as function of p at constant $u = 0.9$ (b).

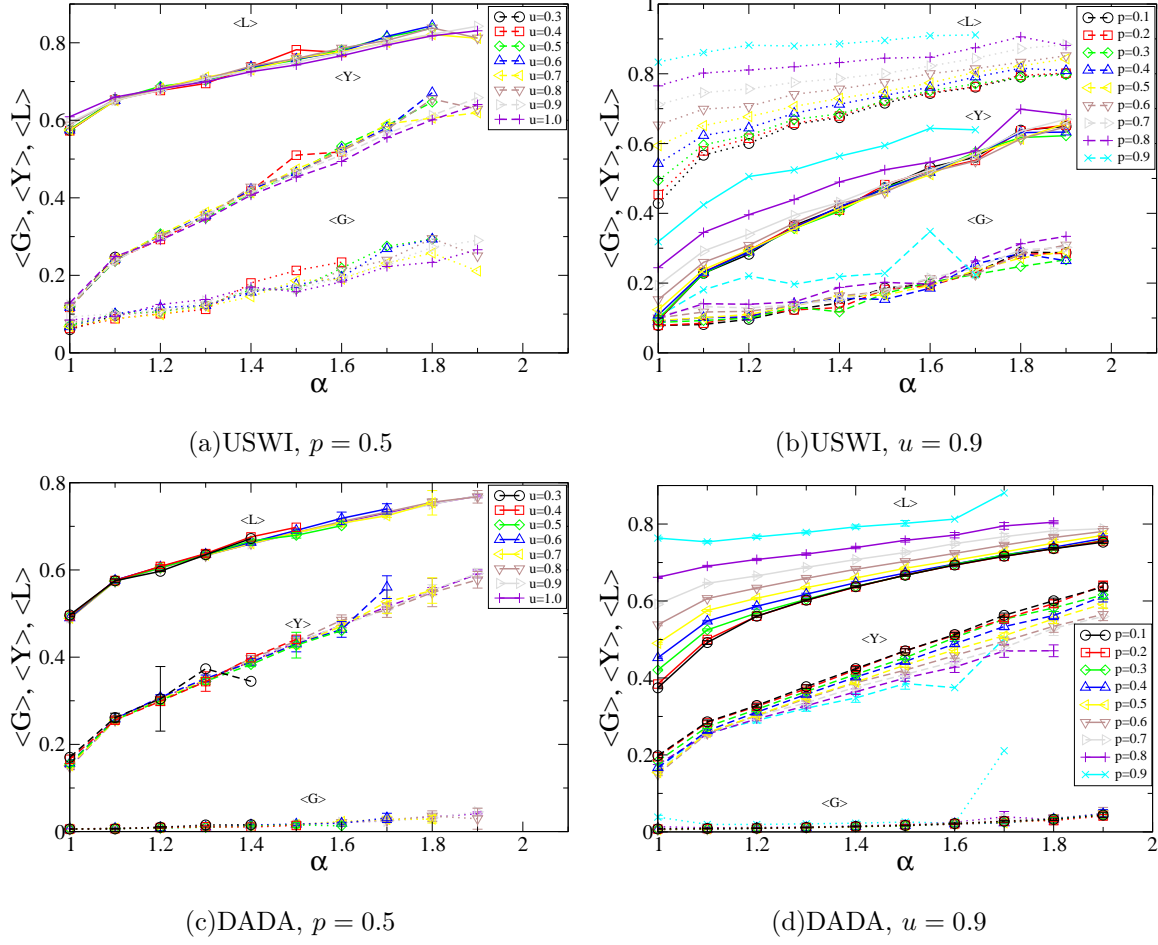


FIG. 10: Behavior of the yield $\langle Y \rangle$, the fraction of nodes in the largest connected component $\langle G \rangle$, and the fraction of survived lines $\langle L \rangle$ averaged only over runs which resulted in large blackouts ($y < 0.8$) as a function of α for different u and a fixed value of $p = 0.5$ (a) USWI model and (c) DADA model, and different p at fixed $u = 0.9$ (b) USWI model and (d) DADA model. The small $\langle G \rangle$ in the DADA model is a feature of the symmetry of the model network and the long lengths of the first links constructed (as necessitated by [3]).

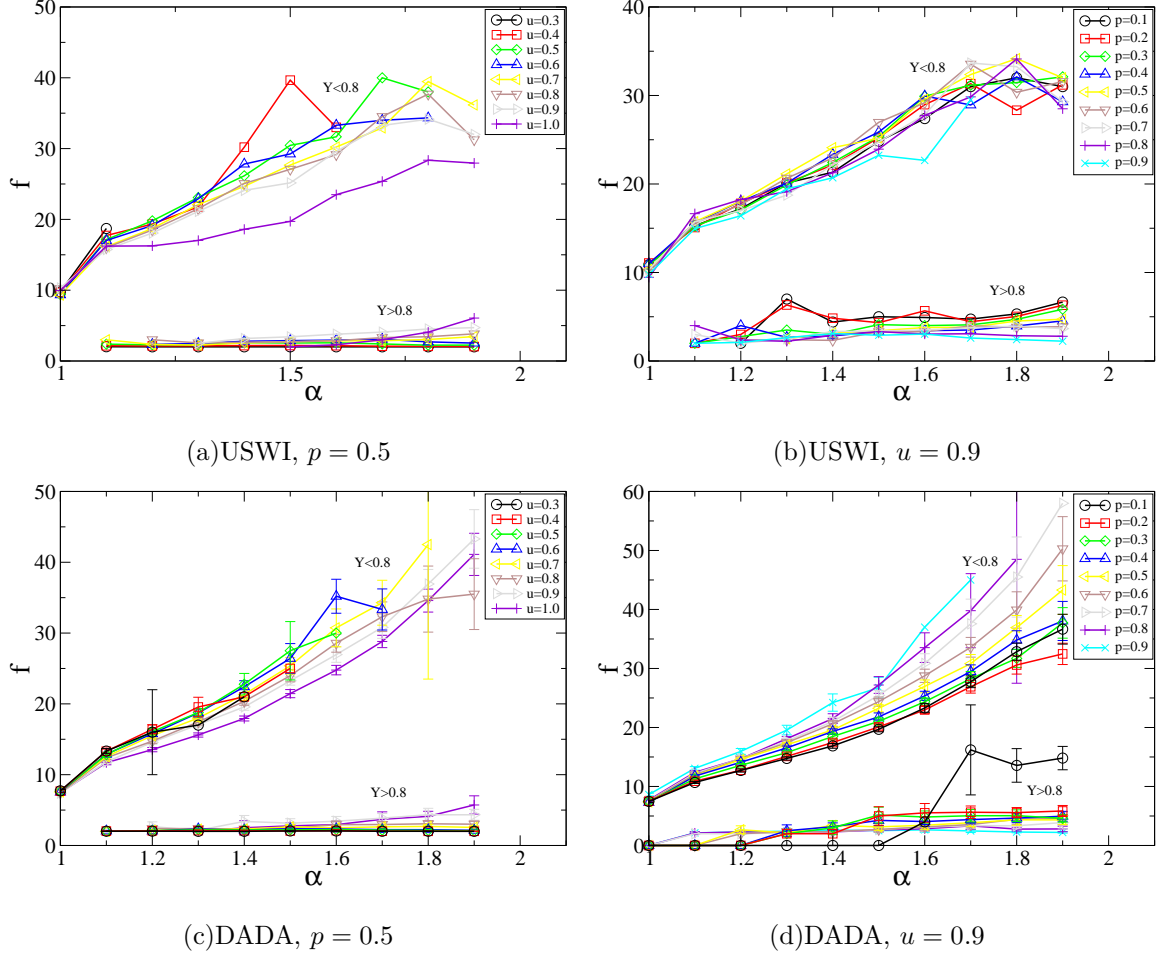


FIG. 11: Dependence of the average duration of the cascade on tolerance α . (a) USWI model and (c) DADA model for different u at $p = 0.5$. (b) USWI model and (d) DADA model for different p at $u = 0.9$. The dependence of the duration of the cascade on both u and p is weak. For each u and p there are two lines: one for cascades resulting in large blackouts with yield $Y < 0.8$, and another for cascades resulting in small blackouts $Y > 0.8$. The duration of the cascades in the large blackout cases is always larger than 10 and is increasing with α , while for the cases with small blackouts the cascades are short. Here we see the cascade slows down with higher α , so higher α means higher resilience and longer latent periods. This shows the resilience of the grid is based on α .

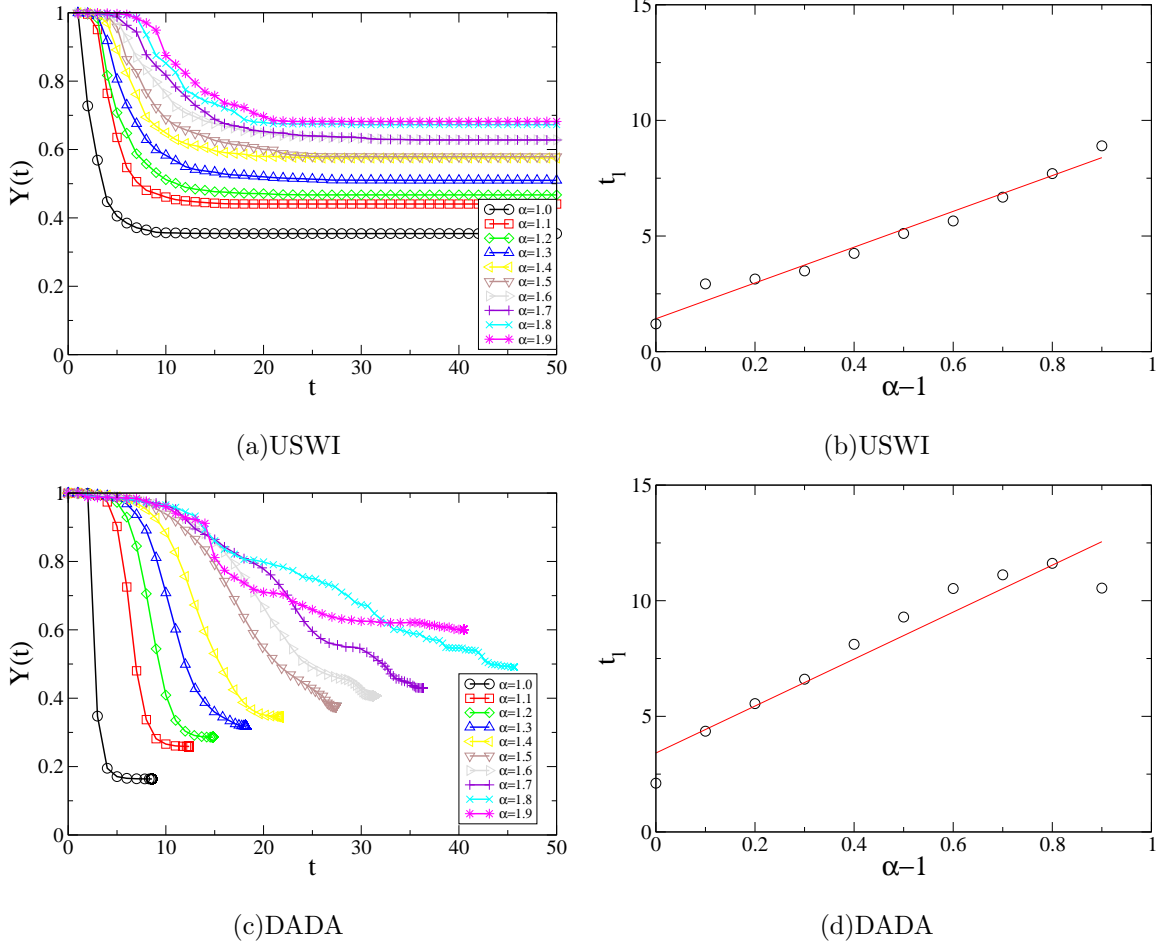


FIG. 12: Decrease in the demanded current as a function of the cascade time step during the cascades resulting in large blackouts for (a) the USWI model and (c) the DADA model. The latent period at the beginning of the cascade, during which there is no significant decrease in the demand, linearly increases with tolerance α for both (b) the USWI model and (d) the DADA model. In both USWI and DADA models $u = 1.0$, $p = 0.9$.

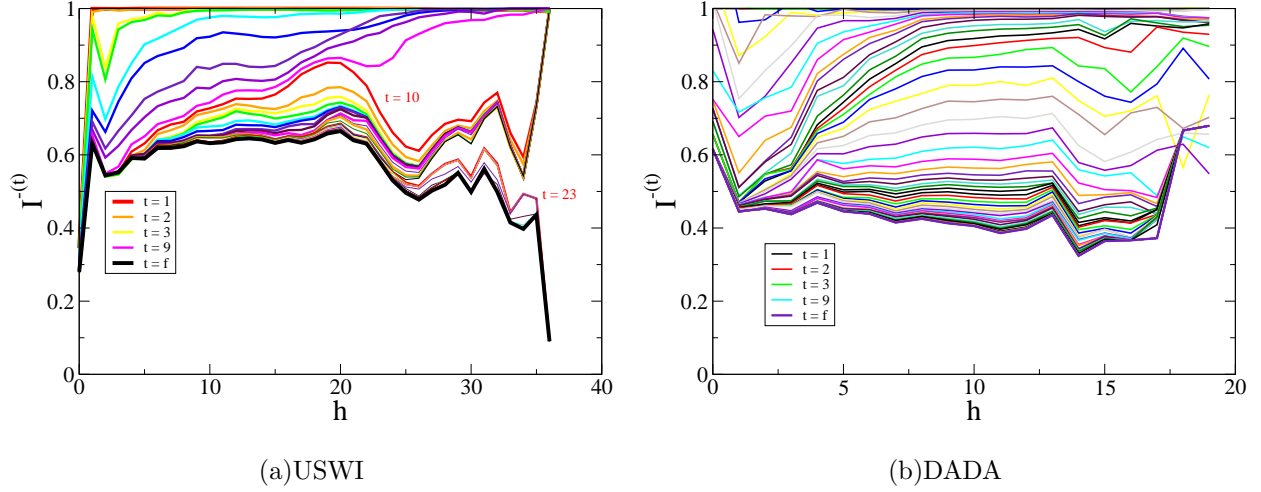


FIG. 13: The fraction of current reaching demand nodes as a function of hop distance in runs resulting in large blackouts for different cascade time steps, with $p = 0.9$ and $\alpha = 1.6$, (a) for the USWI data, and (b) for the DADA model with $\mu = 6$, $\ell = 1.5$.

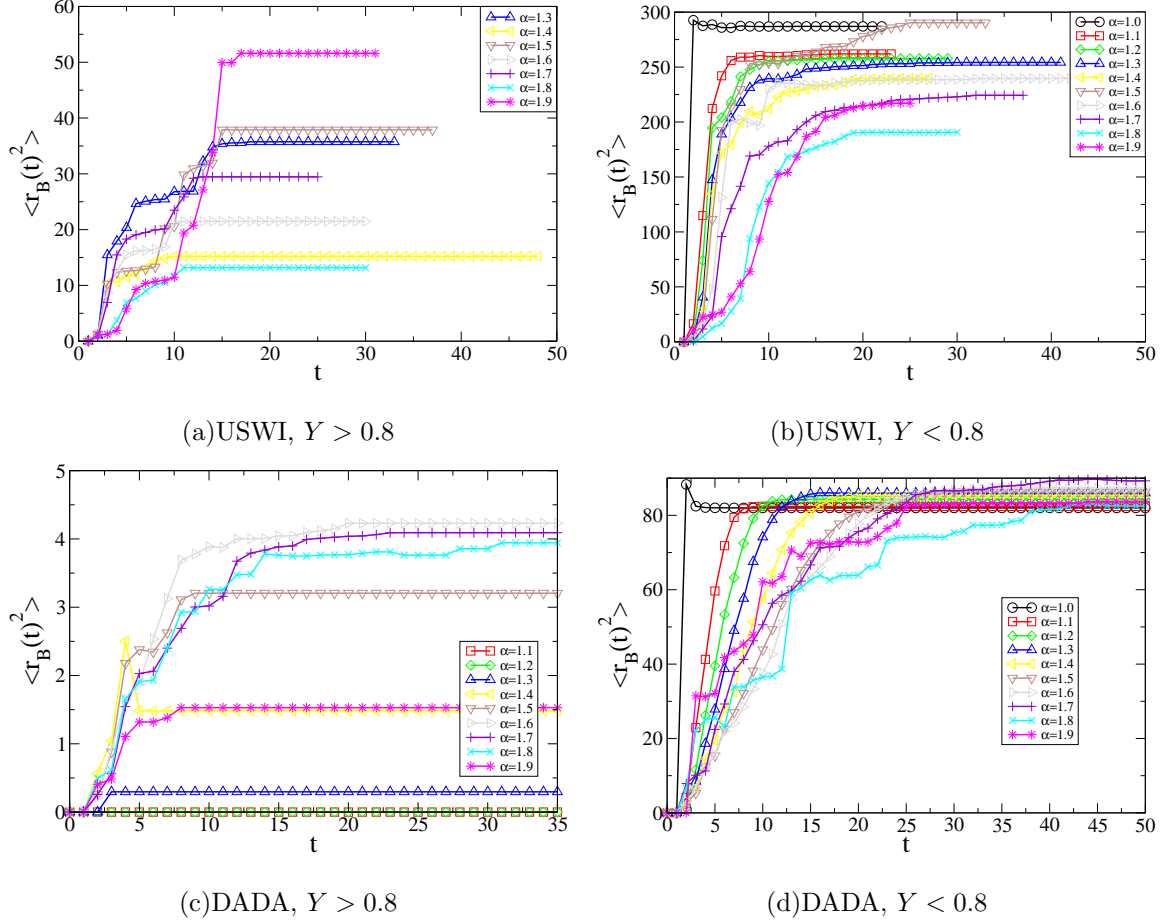


FIG. 14: The averaged behavior of the radius of gyration of the cascading failures in small blackouts $Y > 0.80$ in (a) the USWI model and (c) the DADA model, and large blackouts with $Y < 0.80$ in (b) the USWI model and (d) the DADA model. $r_B(t)^2$ in the DADA model is much smaller than it is in the USWI model due to the different structures of the models and difference in diameters of the networks. The longest distance between any two nodes (i.e. diameter of the network) in the DADA model is ≈ 16 , while in the USWI model it is ≈ 41 . In both models we see that the cascade spreads more quickly for smaller α than for larger α .

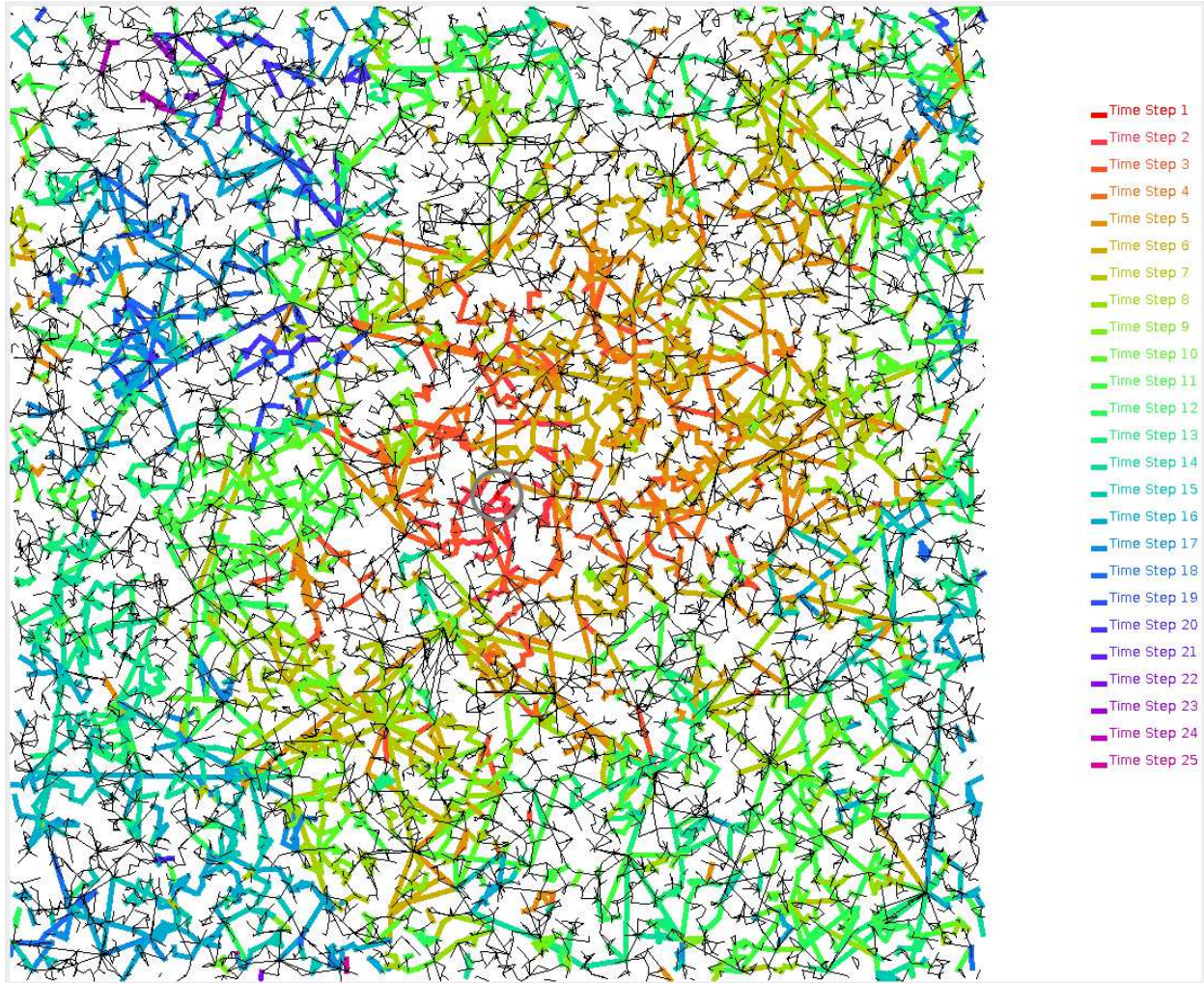


FIG. 15: (Color online) Propagation of a cascade of failures for $\alpha = 1.8$, $p = 0.4$, $u = 1$ in the DADA model with 13135 nodes, $\ell = 1.5$, $\mu = 6$. Lines that failed at different time steps of the cascade are shown with different colors. The line randomly selected to fail due to spontaneous failure or attack is portrayed as the center of the grid and is surrounded by a gray circle.

Appendix A: Solving Flow Equations

In the direct current approximation, the outgoing current from node i through a transmitting line with resistance R_{ij} is $I_{ij} = (V_i - V_j)/R_{ij}$, where V_i and V_j are the potentials of nodes i and j respectively. In addition to the transmitting lines we have to take into account the currents generated by the supply nodes I_i^+ and the currents consumed by the demand nodes I_i^- . In the direct current approximation, it is assumed that the currents $I_i^+ > 0$ and $I_i^- > 0$ are equal to the powers W_i^+ and W_i^- generated by the supply nodes and consumed by the demand nodes, respectively, as explained below. We assume that each supply node i is connected to the source of voltage V_i^+ by a line with high resistance R_i^+ and each demand node i is connected to the ground V_i^- by a line with high resistance R_i^- . For simplicity we assume that $V_i^+ = V$, where V is a constant, and $V_i^- = 0$.

Since the sum of all supply powers must be equal to the sum of all demand powers and resistances R_i^\pm are much larger than R_{jk} of any transmission line, $V_i \approx V/2$. Therefore we can select $R_i^\pm = V/(2W_i^\pm)$ so that the current I_i flowing through each resistance R_i^\pm is approximately equal to the power W_i^\pm . To ensure that $R_i^\pm \gg R_{jk}$, we select $V = M \max_i (W_i^\pm) \max_{jk} (R_{jk})$, where M is a large constant. If M increases, our approximation of the power as current improves in terms of $|I_i - W_i^\pm|$, but the convergence of our algorithm for solving the Kirchhoff equations slows down. We find for $M \approx 10^3$, both accuracy and speed are acceptable.

Thus, the system of the Kirchhoff equations for the grid consists of n linear equations for the potentials of each node V_i

$$V_i \left(\sum_{j \in N(i)} \frac{1}{R_{ij}} \right) - \sum_{j \in N(i)} \frac{V_j}{R_{ij}} = \delta_i^+ I_i^+ - \delta_i^- I_i^-, \quad (\text{A1})$$

where $\delta_i^+ = 1$ or $\delta_i^- = 1$ if a node i is a supply node or a demand node, respectively. Otherwise, $\delta_i^+ = \delta_i^- = 0$.

The determinant of this system is equal to zero, hence solving such a system requires complex linear algebra procedures. In order to be able to use simple relaxation procedures, we must regularize this system by adding positive diagonal terms. We can achieve this by assuming that all the supply nodes are connected to high voltage V with resistance $R_i^+ = M/I_i^+$ and that all the demand nodes are connected to the ground with resistance $R_i^- = M/I_i^-$, where M is a constant. Since units of currents are arbitrary, we decrease I_i^+

and I_i^- by a constant factor of one million; since M remains constant, this ensures that R_i^+ and R_i^- are much larger than any transmission line resistance R_{ij} , so the potential differences within the grid are much smaller than the potential differences between the grid and the source, and between the grid and the ground. Thus, when considering the grid's relation to these external potentials, we can assume all the nodes have approximately the same potential

$$V_g = V \frac{\frac{1}{\sum_i \frac{1}{R_i^-}}}{\frac{1}{\sum_i \frac{1}{R_i^+}} + \frac{1}{\sum_i \frac{1}{R_i^-}}}. \quad (\text{A2})$$

Since due to conservation of charge

$$M \sum_i \frac{1}{R_i^-} = \sum_i I_i^- = \sum_i I_i^+ = M \sum_i \frac{1}{R_i^+}, \quad (\text{A3})$$

$V_g = V/2$. Furthermore, $I_i^+ R_i^+ = M = I_i^- R_i^-$ equals the potential difference between the demand nodes and the ground. Hence, $M = V_g = V/2$. Accordingly, Eq. (A1) can be rewritten as

$$V_i \left(\sum_{j \in N(i)} \frac{1}{R_{ij}} + \delta_i^+ \frac{1}{R_i^+} + \delta_i^- \frac{1}{R_i^-} \right) - \sum_{j \in N(i)} \frac{V_j}{R_{ij}} = \delta_i^+ \frac{V}{R_i^+}. \quad (\text{A4})$$

Now the determinant of this system is not equal to zero due to the presence of $1/R_i^+$ and $1/R_i^-$ terms in the diagonal elements of the system. System (A4) can be rewritten as

$$(\mathbf{I} - \mathbf{B})\vec{V} = \vec{V}_0, \quad (\text{A5})$$

where \mathbf{I} is an identity matrix,

$$b_{ij} = \begin{cases} 0 & \text{for } j \notin N(i) \\ \frac{1}{R_{ij} \left(\sum_{j \in N(i)} \frac{1}{R_{ij}} + \delta_i^+ \frac{1}{R_i^+} + \delta_i^- \frac{1}{R_i^-} \right)} & \text{for } j \in N(i) \end{cases}, \quad (\text{A6})$$

and

$$(\vec{V}_0)_i = \delta_i^+ \frac{V_i^+}{R_i^+ \left(\sum_{j \in N(i)} \frac{1}{R_{ij}} + \delta_i^+ \frac{1}{R_i^+} + \delta_i^- \frac{1}{R_i^-} \right)}. \quad (\text{A7})$$

Since the determinant $|\det \mathbf{B}| < 1$, Eq. (A5) can be solved iteratively:

$$\vec{V}_{m+1} = \mathbf{B}\vec{V}_m + \vec{V}_0 \quad (\text{A8})$$

with the initial condition $V_i = V/2$. Solving these equations, we find voltages $(V)_i$ of each node and the current flow through each line $I_{ij} = |(V_i - V_j)/R_{ij}|$.

Notes:

- To remove a line from the grid, we set its resistance $R_{ij} = \infty$ (i.e., set the conductance to zero to prevent current from traveling through the line, thus the line has been effectively removed).
- We assume that the tolerance of the lines connecting the supply nodes to V and demand nodes to ground is $\alpha^+ = \alpha^- = \infty$, so these lines never fail. Such a model with finite α^+ is much more vulnerable to developing large blackouts than the most conservative variant of shedding that we study.

Appendix B: Expediting Computation

To speed up the iterative algorithm for solving linear equations, we treat separately each disconnected cluster. We pull from the main grid all the relevant information about each cluster and treat them as grids of their own. We cut from these clusters the “dangling ends”, defined (as in [14]) as areas of transmitting nodes connected to the rest of the cluster through one single node. As these “dangling ends” have only transmitting nodes and only one point of connection to the rest of the grid, they have zero current in all their lines. We identify dangling ends by the Hopcroft-Tarjan algorithm for finding biconnected components [17]. We then solve the system in Eq. (A5) for each smaller cluster individually and incorporate the data back into the main grid.

-
- [1] R. Albert and A.-L.Barabási. “Statistical mechanics of complex networks.” *Rev. Mod. Phys.* **74**, 47 (2002).
 - [2] L. de Arcangelis, S. Redner, and H. J. Herrmann, J. “A random fuse model for breaking processes.” *Physique Lett.* **46**, L585 (1985).
 - [3] A. Asztalos, S. Sreenivasan, B. K. Szymanski, and G. Korniss. “Cascading failures in spatially-embedded random networks.” *PloS ONE* 9(1): e84563. 2014.
 - [4] M. Batty and P. Longley. *Fractal Cities: A Geometry of Form and Function* (Academic Press, 1994)

- [5] A.-L. Barabási and R. Albert. “Emergence of Scaling in Random Graphs.” *Science* **286**, 509 (1999).
- [6] A. Bernstein, D. Bienstock, D. Hay, M. Uzunoglu, and G. Zussman. “Power Grid Vulnerability to Geographically Correlated Failures - Analysis and Control Implications.” in *Proc. IEEE INFOCOM’14*, Apr. 2014.
- [7] D. Bienstock. “Optimal control of cascading power grid failures.” *Proc. IEEE CDC-ECC*, Dec. 2011.
- [8] D. Bienstock and A. Verma. “The N - k problem in power grids: New models, formulations, and numerical experiments.” *SIAM J. Optimiz.*, 20(5):2352-2380, 2010.
- [9] B. Bollobás. *Random Graphs* (Academic, London, 1985).
- [10] S. V. Buldyrev, R. Parshani, G. Paul, H. E. Stanley, and S. Havlin. “Catastrophic cascade of failures in interdependent networks.” *Nature (London)* **464**, 1025 (2010).
- [11] B. A. Carreras, V. E. Lynch, I. Dobson, and D. E. Newman. “Critical points and transitions in an electric power transmission model for cascading failure blackouts.” *Chaos* **12**, 985-994 (2002).
- [12] B. A. Carreras, V. E. Lynch, I. Dobson, and D. E. Newman. “Complex dynamics of blackouts in power transmission systems.” *Chaos* **14** 3, 643-652 (2004).
- [13] A. Clauset, C. R. Shalizi, and M. E. J. Newman. “Power-Law Distributions in Empirical Data.” *SIAM Rev.* **51** 4, p.661-703 (2009).
- [14] A. Coniglio. “Thermal Phase Transition of the dilute s-state-Potts and n-vector models at percolation threshold.” *Phys. Rev. Lett.* **46**, 250 (1981).
- [15] I. Dobson and L. Lu. “Voltage Collapse Precipitated by the Immediate Change in Stability When Generator Reactive Power Limits are Encountered.” *IEEE Trans. CAS* vol. 39, No. 9, pp. 762-766. Sept. 1992.
- [16] B. Gungor. *Power System Analysis* (Oxford University Press, USA, 1995).
- [17] J. Hopcroft and R. Tarjan. “Efficient Algorithms for Graph Manipulation.” *Commun. ACM* **16**, 372 (1973).
- [18] Y. Kornbluth, S. Lowinger, G. Cwlich, and S. V. Buldyrev. “Cascading failures in networks with proximate dependent nodes.” *Phys. Rev. E* **89**, 032808 (2014).
- [19] H. A. Makse, S. Havlin, and H. E. Stanley. “Modelling Urban Growth Patterns.” *Nature* **377**, 608-612 (1995).

- [20] S. S. Manna and P. Sen. “Modulated scale-free network in Euclidean space.” *Phys. Rev. E* **66**, 066114 (2002).
- [21] A. E. Motter and Y. Lai. “Cascade-Based Attacks on Complex Networks.” *Phys. Rev. E* **66**, 065102 (2002)
- [22] A. E. Motter. “Cascade Control and Defense in Complex Networks.” *Phys. Rev. Lett.* **93**, 098701(2004).
- [23] NYISO Interim Report August 14, 2003 Blackout, January 8, 2004.
- [24] S. Pahwa, C. Scoglio, and A. Scala. “Abruptness of cascade failures in power grids.” *Sci. Rep.* **4**, 3694 (2014).
- [25] A. Pinar, J. Meza, V. Donde, and B. Lesieutre. “Optimization strategies for the vulnerability analysis of the electric power grid.” *SIAM J. Optimiz.*, 20(4):1786-1810, 2010.
- [26] Platts. “GIS Data.” <http://www.platts.com/Products/gisdata>.
- [27] D. C. Rapaport. *The Art of Molecular Dynamics Simulation. 2nd ed.* (Cambridge University Press, 2004).
- [28] “Report of the enquiry committee on grid disturbance in the Northern region on 30th July 2012 and in Northern, Eastern and North-Eastern region on 31st July 2012.” Aug. 2012.
- [29] “Report on the Grid Disturbance on 30th July 2012 and Grid Disturbance on 31st July 2012.” 2012.
- [30] S. Soltan, D. Mazauric, and G. Zussman. “Cascading Failures in Power Grids — Analysis and Algorithms.” *in Proc. ACM e-Energy '14*, June (2014).
- [31] The Federal Energy Regulatory Commission (FERC) and the North American Electric Reliability Corporation (NERC). “Arizona-Southern California Outages on September 8, 2011.” 2012.
- [32] “U.S-Canada Power System Outage Task Force report on the August 14, 2003 blackout in the United States and Canada: Causes and recommendations.” 2004.
- [33] U.S FERC, DHS, and DOE. “Detailed technical report on EMP and severe solar flare threats to the U.S. power grid.” Oct. 2010.
- [34] R. Xulvi-Brunet and I. M. Sokolov. “Evolving networks with disadvantaged long-range connections.” *Phys. Rev. E* **66**, 026118 (2002).
- [35] S. Zapperi, P. Ray, H. E. Stanley, and A. Vespignani. “First-Order Transition in the Breakdown of Disordered Media.” *Phys. Rev. Lett.* **78**, 1408 (1997).